A NEW APPROACH FOR THE CHARACTERIZATION OF THE PORE STRUCTURE OF DUAL POROSITY ROCKS

Christos D. Tsakiroglou[1,*], Marios A. Ioannidis[2], Edison Armitharaj[2], Olga Vizika[3]

[1]FORTH / ICE-HT, Stadiou Street, Platani, P.O. Box 1414, GR – 26504 Patras, Greece
[2]Department of Chemical Engineering, University of Waterloo, Ontario N2L 3G1, Canada
[3]Institut Francais du Petrole, 1&4 Avenue de Bois-Preau, 92852 Rueil-Malmaison, France

This paper was prepared for presentation at the International Symposium of the Society of Core Analysts held in Trondheim, Norway 12-16 September, 2006

ABSTRACT

For the realistic representation of the pore space of dual porosity rocks, a new method of pore structure characterization is developed by combining experimental Hg intrusion / retraction curves with BSEM images and inverse modeling algorithms. The autocorrelation function of BSEM images is combined with the surface fractal dimension resulting from the very high pressure Hg intrusion (MIP) data to derive an extended scattering intensity (SANS) function which provides a volume-based pore body radius distribution (PBRD). The volume-based PBRD is fitted with a multimodal number-based PBRD consisting of two component distributions: one representing the macroporosity and another one representing the microporosity. Based on arguments of percolation theory, analytical mathematical models are developed to describe the Hg intrusion in and retraction from dual pore networks in terms of the complete PBRD, pore throat radius distribution of macroporosity (PTRD), drainage accessibility functions (DAFs) of both porosities, and imbibition accessibility functions (IAFs) of both porosities. Inverse modeling of the Hg intrusion data set enables us to estimate the PTRD and DAFs. Inverse modeling of the Hg retraction datasets enables us to estimate a set of primary and secondary IAFs. The method is demonstrated with the characterization of the pore structure of three outcrop samples of carbonates and sandstones. Analytic approximate equations developed by using the critical path analysis (CPA) of percolation theory enable us to calculate explicitly the absolute permeability and formation factor of the porous rocks from the estimated parameters (PBRD, PTRD, DAF) of the macroporosity.

INTRODUCTION

Many methods have been developed to analyze the pore structure properties at the various ranges of length scales, but yet no single method can probe five or more orders of magnitude of the pore length scale, as required. For instance back-scattered scanning

* Corresponding author, e-mail: ctsakir@iceht.forth.gr, Tel.: 2610 965212, Fax: 2610 965223

electron microscopy (BSEM) is suitable to provide statistically significant microstructure data at length scales from several mm to a few μm [5]. Indirect imaging methods like the small-angle neutron scattering and x-ray scattering (SANS and SAXS) yield the volume-averaged Fourier transform of the two-point correlation function at length scales ranging from 1nm to 10 μm [8]. Mercury porosimetry is widely used to probe the pore space in the range 20 nm to 200 μm, but instead of the pore size distribution, this method provides the distribution of pore volume that is accessible to Hg through pore throats of different size [4,11,12]. Combining Hg porosimetry data with serial-sectioning analysis of double porecasts and mechanistic simulators at the pore-network scale, information concerning topological, geometrical and correlational properties of the pore space can be extracted [13]. Geometrical and topological parameters of nanoporous materials can be extracted from the N2 adsorption-desorption isotherms [6]. The inverse modeling of Hg porosimetry curves and N2 sorption isotherms seems a well-promising method for the characterization of the structure of nanoporous materials [14]. When applied to macroporous materials, N2 adsorption/condensation detects the fractal characteristics of the solid-void interface in a manner that is consistent to SANS/SAXS measurements in porous rocks [2]. The statistical fusion of SANS and BSEM data and their subsequent interpretation in terms of a polydispersed spherical pore model was proposed as a potential method to characterize the pore structure of sandstones and detect pore sizes in the range 1nm -1μm, including the fractal and Euclidean pore space, as well [10]. The method was modified and information normally provided by SANS measurements has been substituted approximately by a fractal scaling law using estimates of the surface fractal dimension from mercury intrusion porosimetry [1,3].

In the present work, a new method of pore structure characterization that is able to probe pore sizes over a very broad range (from nm to mm) is developed and demonstrated with application to dual porosity outcrop samples of sandstones and carbonates. BSEM images and high pressure Hg intrusion (MIP) data are employed to estimate the pore-body radius distributions (BPRD) of the macroporosity and microporosity. Experimental Hg intrusion /retraction curves are introduced into inverse modeling algorithms to estimate the pore throat radius distribution (PTRD) of the primary porosity along with the drainage (DAF) and imbibition (IAF) accessibility functions of the macroporous and microporous networks. Using the critical path analysis (CPA) of percolation theory, analytical relationships are suggested to calculate the permeability and formation factor of porous rocks from the parameters (PBRD, PTRD, DAF) characterizing the macroporosity

ESTIMATION OF THE PBRD FROM BSEM IMAGES AND MIP DATA

A porous medium can be described in terms of a phase function $Z(\mathbf{x})$ taking the value of unity if $\mathbf{x}$ points to void and zero otherwise. The first two moments of the phase function are readily accessible from binary BSEM images [5] and correspond to the porosity, ϕ, and autocorrelation function $S_2(\mathbf{r})$:

$$\phi = \langle Z(\mathbf{x}) \rangle \quad (1)$$

$$S_2(\mathbf{r}) = \langle Z(\mathbf{x}) Z(\mathbf{x}+\mathbf{r}) \rangle \quad (2)$$

where $\mathbf{r}$ is a lag vector. For isotropic media the autocorrelation function depends only on the modulus of the lag vector, namely $S_2(\mathbf{r}) = S_2(r)$. The autocorrelation function $S_2(r)$ of a binary BSEM image and the scattering intensity $I(Q)$ measured from SANS experiments are a Fourier transform pair. $I(Q)$ data in the small-Q (large-r) range, which cannot be obtained from SANS measurements, can be computed via Eq.(2) from $S_2(r)$. It is on this basis that SANS and BSEM imaging information may be combined to obtain the $I(Q)$ in the range $10^{-7} < Q < 10^{-1} A$ [10]. The fusion of structural information from BSEM and SANS enables the determination of the pore size distribution in the range 0.001 μm<r<1 mm [10]. Assuming that the pore space can be represented by an assembly of independent spherical pores with an arbitrary distribution $f_s(r)$ of radii r, the scattering intensity per unit volume is given by

$$I(Q) = (\Delta\rho)^2 \frac{\phi}{\langle V_r \rangle} \int_{R_{min}}^{R_{max}} V_r^{\,2} f_s(r) F_s(Qr) dr \quad (3)$$

where R_{max} and R_{min} are the maximum and minimum pore radii, respectively, $V_r = V(r) = (4/3)\pi r^3$ is the volume of a sphere of radius r, $\langle V_r \rangle$ is the average pore volume, $f_s(r)$ is the probability density of the PBRD, and $F_s(Qr)$ is the structure factor for a sphere of radius r [3,9,10]. The function $f_s(r)$ is determined by inversion of the extended $I(Q)$ data using Eq.(3). In the absence of SANS data, the missing $I(Q)$ curve in the large Q-range (small pore length scales) may be reconstructed approximately by using the surface fractal dimension that is estimated from the very high pressure MIP data according to the scaling relation $-dS_{Hg}/dr \propto r^{2-D_s}$ [3]. According to the power law $I(Q) \propto Q^{D_s-6}$, the $I(Q)$ curve is extrapolated over the large Q-range and is inverted to derive the complete pore size distribution [3].

MATHEMATICAL MODELS OF HG INTRUSION / RETRACTION

Drainage and Imbibition Accessibility functions

From pore network simulations it is well known that the pore space topology and spatial pore size correlations are introduced implicitly into the site accessibility functions of primary drainage relating the fraction of the sites (pore bodies) that are accessible to Hg, Y_{s0}, with the fraction of bonds (pore throats) that are "open" to it, q_b [14]. Pore network simulations have revealed that drainage accessibility functions (DAFs) can be described satisfactorily by sigmoid curves of the form [7,14]

$$Y_{s0}(q_b) = \frac{(1+a_0)e^{-b_0(1-q_b)/q_b}}{1+a_0 e^{-b_0(1-q_b)/q_b}} \quad (4)$$

Details on the modeling of Hg intrusion as an invasion percolation process are reported elsewhere [14].

In general, the pore space is not filled completely by mercury at the maximum pressure of intrusion. Instead, several mercury menisci of high curvature remain in regions of very small effective radii (e.g. pore-wall roughness, pore corners, etc). These menisci act as nuclei from which mercury start retracting from the pore network [4,11,12]. The synergistic effect of the pore-scale mechanisms on the overall process is reflected in the imbibition accessibility functions. These functions differ from the corresponding ones of drainage particularly with respect to their final part which is associated with the residual non-wetting fluid saturation. A detailed description of the modeling of Hg retraction as a site percolation process is reported elsewhere [7]. The imbibition accessibility function (Hg retraction) is defined with reference to the wetting fluid (vacuum) and expresses the fraction of sites (pore bodies) occupied by the wetting fluid, X_{sw}, as a function of the corresponding fraction of sites, q_{sw} that are "open" to it. The imbibition accessibility function (IAF) can be approximated by

$$X_{sw} = \frac{h_s(1+a_s)e^{-b_s(1-q_{sw})/(q_{sw}-q_{swf})}}{1+a_s e^{-b_s(1-q_{sw})/(q_{sw}-q_{swf})}} \quad (5)$$

where q_{swf} is the value of q_{sw} at the end of Hg intrusion. Depending on whether $q_{swf} \cong 0$ (at the maximum high MIP pressure) or $q_{swf} > 0$ (at the maximum low MIP pressure) the primary or secondary accessibility function is obtained.

Percolation Models of Hg Intrusion / Retraction in Dual Pore Networks

A pore structure with pore sizes extending from large to very small length scales can be regarded as a dual pore network consisting of a "primary" network of large (macro-) pores interbedded by a "secondary" network of small (micro-) pores (Fig.1). Two accessibility functions (DAFs) are required to describe the effects of the topology of macroporosity, $Y_{s0}(q_b)$, and microporosity, $Y_{s2}(q_{s2})$ on Hg intrusion. Moreover, the micropores become accessible to Hg via Hg-occupied pores of the macroporosity. No throats are considered for the microporosity, the DAF of which has the form

$$Y_{s2}(q_{s2}) = q_{s2}\frac{(1+a_2)e^{-b_2(1-q_{s2})/q_{s2}}}{1+a_2 e^{-b_0(1-q_{s2})/q_{s2}}} \quad (6)$$

where Y_{s2} is the fraction of pore bodies that are accessible to Hg and q_{s2} is the fraction of the pore bodies that are open to Hg. The geometry of the pore space is described by the PBRD, $f_{s1}(r)$, and PTRD, $f_b(r)$, of the macroporosity along with the PBRD, $f_{s2}(r)$, of the microporosity. Taking into account that the micropores become accessible to Hg

through Hg-occupied macropores, Hg intrusion in dual pore networks is described by the analytical relationship

$$S_{Hg}(P_c) = \frac{c_s \frac{Y_{s0}(q_b)}{q_s} \int_{r_s}^{\infty} f_{s1}(r) V_s(r) dr + (1-c_s) \frac{Y_{s0}(q_b)}{q_s} \frac{Y_{s2}(q_{s_2})}{q_{s_2}} \int_{r_s}^{\infty} f_{s2}(r) V_s(r) dr}{c_s \int_0^{\infty} f_{s1}(r) V_s(r) dr + (1-c_s) \int_0^{\infty} f_{s2}(r) V_s(r) dr} \quad (7a)$$

where

$$P_c = 2\gamma_{Hg} \cos\theta_I / r_s \quad (7b)$$

Depending on the final state of Hg intrusion, the effects of the pore space topology on Hg retraction (imbibition) are reflected in two pairs of imbibition accessibility functions (IAFs): (1) the primary accessibility functions of macroporosity and microporosity, when initiating with the pore space almost entirely occupied by Hg; (2) the secondary accessibility functions of macroporosity and microporosity when initiating with the pore space partially occupied by Hg. Hg retraction from a dual pore network is described by the analytical relationship

$$S_{Hg}(P_c) = 1 - \frac{\begin{aligned} & c_s \left[1 - \frac{Y_{s0}(q_{bf})}{q_{sf}}\right] \int_{r_s}^{\infty} f_{s1}(r) V_s(r) dr + (1-c_s) \left[1 - \frac{Y_{s0}(q_{bf})}{q_{sf}} \frac{Y_{s2}(q_{s2f})}{q_{s2f}}\right] \int_{r_s}^{\infty} f_{s2}(r) V_s(r) dr \\ & + c_s \left\{1 - \frac{Y_{s0}(q_{bf})}{q_{sf}} \left[1 - \frac{X_{sw}(q_{sw})}{q_{sw}}\right]\right\} \int_{r_{sf}}^{r_s} f_{s1}(r) V_s(r) dr + \\ & (1-c_s) \left\{1 - \frac{Y_{s0}(q_{bf})}{q_{sf}} \frac{Y_{s2}(q_{s2f})}{q_{s2f}} \left[1 - \frac{X_{sw2}(q_{sw2})}{q_{sw2}}\right]\right\} \int_{r_{sf}}^{r_s} f_{s2}(r) V_s(r) dr \\ & + c_s \int_0^{r_{sf}} f_{s1}(r) V_s(r) dr + (1-c_s) \int_0^{r_{sf}} f_{s2}(r) V_s(r) dr \end{aligned}}{c_s \int_0^{\infty} f_{s1}(r) V_s(r) dr + (1-c_s) \int_0^{\infty} f_{s2}(r) V_s(r) dr}$$

(8a)

where

$$P_c = 2\gamma_{Hg} \cos\theta_R / r_s \quad (8b)$$

PARAMETER ESTIMATION

The dual pore network (Fig.1) is regarded as a pore system consisting of a macroporous network with PBRD, $f_{s1}(r)$, and a microporous network with PBRD, $f_{s2}(r)$. The two PBRDs are components of the complete PBRD that is given by

$$f_s(r) = c_s f_{s1}(r) + (1-c_s) f_{s2}(r) \quad (9)$$

where c_s and $1-c_s$ are the contribution fractions of $f_{s1}(r)$ and $f_{s2}(r)$ to $f_s(r)$. The full set of the parameters of $f_s(r)$ are estimated with non-linear fitting of the volume-based cumulative PBRD, $F_V(r)$, resulting from the fusion of BSEM and MIP data (Fig.2). The PTRD, $f_b(r)$, along with the drainage accessibility functions of the macroporosity, $Y_{s0}(q_b)$, and microporosity, $Y_{s2}(q_{s2})$, are estimated with the non-linear fitting of the Hg intrusion percolation model, Eq.(7), to corresponding experimental datasets. Finally, the primary and secondary imbibition accessibility functions of the macroporous, $X_{sw0}(q_{sw})$, and microporous, $X_{sw2}(q_{sw2})$, networks are estimated with the non-linear fitting of the Hg retraction percolation model, Eq.(8), to the high and low pressure Hg retraction curves, respectively. The non-linear parameter estimation was done by using the Bayesian estimator of ATHENA visual workbench software [7,14].

RESULTS AND DISCUSSION

Porecasts of samples from two sandstones (palatinate, goui) and three carbonates (cj, lavoux, st-maximin) were constructed by impregnating Spurr resin (ERL-4206) in the pore space under a confining pressure of 10 bars. BSEM images of well-polished cross-sections of pore casts (Fig.2) were employed to calculate the autocorrelation function. The low (10-350 kPa) and high (0.1-400 MPa) pressure Hg intrusion / retraction curves of rock samples were measured in a PoreMaster 60 (Quantachrome) mercury porosimeter. The autocorrelation function was combined with high pressure MIP data to derive the complete scattering intensity curve, the inversion of which derived the volume-based cumulative PBRD (Fig.3). When no fractal behaviour was detected, instead of using the MIP data, results from the analysis of BSEM images taken at two magnifications were fused to get the complete PBRD (Fig.3c).

The results of the application of the methodology to three samples (cj4, st-maximin, goui) are shown in Figs. 4, 5 and 6, respectively. Both the Hg intrusion and retraction curves are predicted satisfactorily by the analytical percolation models at the estimated parameter values (Figs. 4a,5a,6a). The PTRD, $f_b(r)$, and PBRD, $f_{s1}(r)$, of the macroporosity overlap significantly (Figs.4b,5b,6b), whereas the PBRD of the microporosity extends to length scales smaller than those of the PTRD. It should be pointed out that the contribution fraction, c_s, of the number-based PBRD of the macroporosity is quite small compared to the contribution fraction, $1-c_s$, of the PBRD of microporosity (Figs.4,5,6). This means that the number of macro-pores is very low compared to the number of micro-pores, a behaviour that can easily be confirmed from BSEM images by focusing on an area at various magnifications. The very wide DAFs of the macroporosity along with the relatively low value of percolation threshold, q_{bc0} (calculated at the inflection point of DAF, [14]) is indicative of the very strong spatial pore size correlations [4,14] (Figs. 4c,5c,6c). For carbonates, the DAF of the microporosity (Fig.4c,5c) is a straight line ($Y_{s2} \cong q_{s2}$). This means that all pores are

accessible to Hg at the corresponding P_c value, without being "shadowed" by smaller pores. In other words, the micropores in carbonates are arranged in cascade layers of progressively smaller pore sizes, and hence the microporosity has the morphology of a fractal-like structure. Instead, this is not the case for the sandstone (Fig.6c) where the pore accessibility is limited.

The IAFs were plotted in the form of relations of the fraction of pores that are accessible to wetting fluid (vacuum) with the capillary pressure (Figs.4d, 5d, 6d). It is evident that the range of capillary pressures and the fraction of the pore volume that empties during Hg retraction (Figs.4a,5a,6a) is governed by the position and width of the primary and secondary IAFs of the macroporosity, X_{sw} (Figs.4d,5d,6d). In carbonates (Figs.4,5), the relatively low residual Hg saturation (Figs.4a,5a) is trapped in a small fraction of large macropores (Figs.4d,5d). In the sandstone, the relatively high residual Hg saturation (Fig.6a) is associated with the small fraction of macropores that empty at the lowest capillary pressure (Fig.6d). Probably this is due to a high frequency of snap-off events in throats [11] because of a high pore-to-throat aspect ratio implied by the weak overlapping of PBRD and PTRD in macroporosity (Fig.6b).

Critical Path Analysis

The hydraulic or electrical conductivity of a pore system with broad throat and pore size distribution (Fig.4b,5b,6b) is governed by a critical (hydraulic or electrical) pore conductance, g_c, which is defined by the condition that all pores with conductance greater than g_c create a network spanning cluster transferring most of the flow or current. This critical conductance g_c depends on structural characteristics (e.g. pore shape, pore size distribution, connectivity, dimensionality, etc) of the pore space and critical path analysis (CPA) is used to calculate the corresponding critical pore dimensions [15]. According to CPA [15] all conductances with values greater than g_c are set equal to g_c, while all conductances smaller than g_c are set equal to zero. In order to derive expressions for the permeability and formation factor, the hydraulic and electrical conductance of an axisymmetric sinusoidal unit cell is coupled with the estimated PBRD, PTRD, and DAF of the macroporosity (Figs.4,5,6).

The permeability of a (macroporous) network spanning cluster is approximated by

$$k = g_{huc}\left(R_{bh}, R_{sh}\right)\mu \frac{2R_{sh}\phi\varepsilon_p\left[S_{Hg1}\left(R_{bh}\right) - S_{Hg1c}\right]}{\pi\left[\left(R_{bh} + R_{sh}\right)/2\right]^2} \tag{11}$$

where, μ is the fluid viscosity, $g_{huc}\left(R_{bh}, R_{sh}\right)$ is the hydraulic conductance of a sinusoidal cell consisting of a throat of radius R_{be} and the segments of two pore bodies of radius R_{se}, ϕ is the total porosity, ε_p is the fraction of the total pore volume belonging to macroporosity, S_{Hg1} is the Hg saturation in the macroporosity, and $S_{Hg1c} = S_{Hg1}\left(r_b = R_{bc}\right)$ is the corresponding Hg saturation at the percolation threshold, $q_{bc0} = q_b\left(r_b = R_{bc}\right)$.

Likewise, the formation factor of a network spanning cluster is approximated by

$$F = \frac{\pi c_w \left[\left(R_{be} + R_{se}\right)/2\right]^2}{2R_{se}\phi\varepsilon_p g_{euc}\left(R_{be}, R_{se}\right)\left[S_{Hg1}\left(R_{be}\right) - S_{Hg1c}\right]} \quad (12)$$

where c_w is the brine conductivity, and $g_{euc}\left(R_{be}, R_{se}\right)$ is the electrical conductance of a cell consisting of a throat of radius R_{be} and the segments of two pore bodies of radius R_{se}.

The hydraulic critical path (HCP) is determined from Eq.(11) by calculating the throat radius, $R_{bh,max}$ where the permeability is maximized, namely $\left(dk/dR_{bh}\right)_{R_{bh}=R_{bh,\max}} = 0$. Respectively, the electrical critical path (ECP) is determined from Eq.(12) by calculating the throat radius $R_{be,max}$ where the formation factor is minimized, namely $\left(dF/dR_{be}\right)_{R_{be}=R_{be,\min}} = 0$. By using the PBRD, PTRD, and DAF of the macroporosity of the investigated rocks (Figs4,5,6), the absolute permeability of the HCP, $k_{CP,max}$ as well as the formation factor of the ECP, $F_{CP,\min}$, were determined and are given in Table 1.

CONCLUSIONS

A method is presented for the characterization of the pore structure of dual porosity rocks in terms of the pore-body and pore-throat size distributions (PBRD and PTRD) of macroporosity, the pore-body size distribution (PBRD) of microporosity, and the drainage & imbibition accessibility functions (DAF and IAF) of macroporosity, and microporosity. The method combines data resulting from the analysis of 2-D BSEM images with Hg intrusion-retraction datasets and inverse modeling algorithms. Beyond the pore size distributions (PBRD and PTRD) the method enables us to estimate the accessibility functions that quantify implicitly the pore connectivity and spatial pore size correlations. The geometrical and topological parameters of the pore space can be used to calculate explicitly the single-phase (permeability, formation factor) transport properties of dual porosity media, without the necessity of using complex deterministic pore network models.

ACKNOWLEDGEMENTS

This work was supported by the General Secretariat for Research and Technology / Ministry of Development (Greece) and EGIDE (France), in the course of bilateral cooperation R&D program “PLATON” (Decision No: 19557/17-12-2001), as well as by European Commission, in the course of 6th Framework Program, Subprogram: “Global Change and Ecosystems”, contract number: SSPI-CT-2003-004017-STRESOIL.

REFERENCES

1. Armitharaj, E., M.A. Ioannidis, and I.F. Macdonald, "Statistical synthesis of image analysis and mercury porosimetry for multiscale pore structure characterization", *Proceeding of the 2003 Annual Symposium of the Society of Core Analysts*, Paper SCA2003-10, pp.111-122, Pau, France, 21-24 Sept. 2003.
2. Broseta, D., L. Barre, O. Vizika, N. Shahidzadeh, J.P. Guibaud, and S. Lyonnard, "Capillary condensation in a fractal porous medium", *Phys. Rev. Lett.* (2001) **86**, 5313-5316.
3. Hu, B., H. Han, M.A. Ioannidis, E.S. Armitharaj, and Y. Yan, "Pore structure characterization of core samples from Daqing oilfield by a synthesis of mercury porosimetry and image analysis", *Proceeding of the 2005 Annual Symposium of the Society of Core Analysts*, Paper SCA2005-22, Toronto, Canada, 21-25 August 2005.
4. Ioannidis, M.A., and I. Chatzis, "Network modeling of pore structure and transport properties of porous media", *Chem. Eng. Sci.* (1993) **48**, 951-972.
5. Ioannidis, M.A., M.J. Kwiecien, and I. Chatzis, "Statistical analysis of the porous microstructure as a method for estimating reservoir permeability", *J. Pet. Sci. & Eng.* (1996) **16**, 251-261.
6. Liu, H., L. Zhang, and N.A. Seaton, "Analysis of sorption hysteresis in mesoporous solids using a pore network model", *J. Colloid Interface Sci.* (1993) **156**, 285-293.
7. Nikolakis, V., and C.D. Tsakiroglou, "Interpretation of the transport properties of α-Al2O3 supports in terms of pore structure characteristics", *Ind. Eng. Chem. Res.* (2005) **44**, 2333-2342.
8. Radlinski, A.P., E.Z. Radlinska, M. Agamalian, G.D. Wignall, P. Lindner, and O.G. Randi, "Fractal geometry of rocks", *Phys. Rev. Lett.* (1999) **82**, 3078-3081.
9. Radlinski, A.P., C.J. Boreham, P. Lindner, O. Randi, G.D. Wignall, A.L. Hinde, and J.M. Hope, "Small-angle neutron scattering signature of oil generation in artificially and naturally matured hydrocarbon source rocks", *Organic Geochemistry* (2000) **31**, 1-14.
10. Radlinski, A.P., M.A. Ioannidis, A.L. Hinde, M. Hainbuchner, M. Baron, H. Rauch, and S.R. Kline, "Angstrom-to-millimeter characterization of sedimentary rock microstructure**",** *J. Colloid Interface Sci.* (2004) **274**, 607-612
11. Tsakiroglou, C.D. and A.C. Payatakes, "A new simulator of mercury porosimetry for the characterization of porous materials", *J. Colloid Interface Sci.* (1990) **137**, 315-339.
12. Tsakiroglou, C.D. and A.C. Payatakes, "Pore-wall roughness as a fractal surface and theoretical simulation of mercury intrusion/retraction in porous media", *J. Colloid Interface Sci.* (1993) **159**, 287-301.
13. Tsakiroglou, C.D. and A.C. Payatakes, "Characterization of the pore structure of reservoir rocks with the aid of serial sectioning analysis, mercury porosimetry and network simulation", *Adv. Water Resour.* (2000) **23**, 773-789.
14. Tsakiroglou, C.D., V.N. Burganos, and J. Jacobsen, "Pore structure analysis by using nitrogen sorption and mercury intrusion data", *AIChE J.* (2004) **50,** 489-510.
15. Tsakiroglou, C.D., "Determination of the transport properties of single fractures with the aid of critical path analysis", *Ind.l & Eng. Chem. Res.* (2002) **41**, 3462-3472.

Table 1. Transport properties and critical throat / pore dimensions calculated with the CPA

Rock sample	$R_{bh,\max}$ (μm)	$R_{sh,\max}$ (μm)	$k_{CP,\max}$ (mD)	$R_{be,\min}$ (μm)	$R_{se,\min}$ (μm)	$F_{CP,\min}$
cj4	5.35	11.4	30.2	0.18	0.8	51.5
st-maximin	11.3	20.8	2189	6.15	15.6	6.55
goui	5.5	11.2	174.7	2.35	7.9	17.8

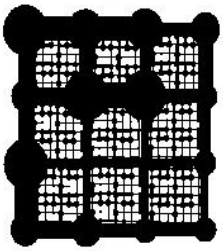

Figure 1. Conceptual model of a dual pore network.

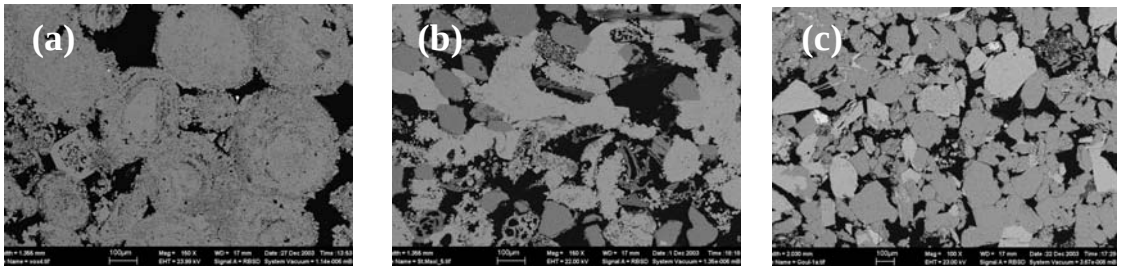

Figure 2. BSEM images: (a) cj4 (carbonate). (b) st-maximin (carbonate). (c) goui (sandstone)

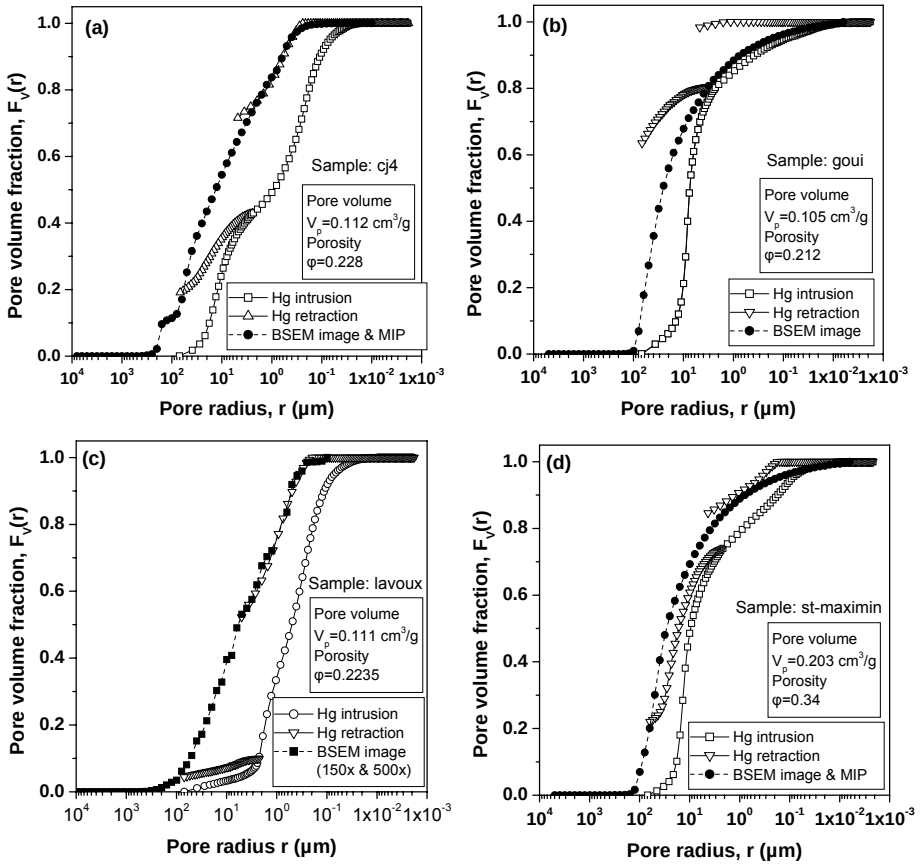

Figure 3. Volume-based complete PBRD from BSEM images & MIP data as compared with the measured Hg intrusion & retraction curves. (a) cj4 (D_s=2.01-2.89). (b) goui (D_s=2.6). (c) lavoux. (d) st-maximin (D_s=2.6).

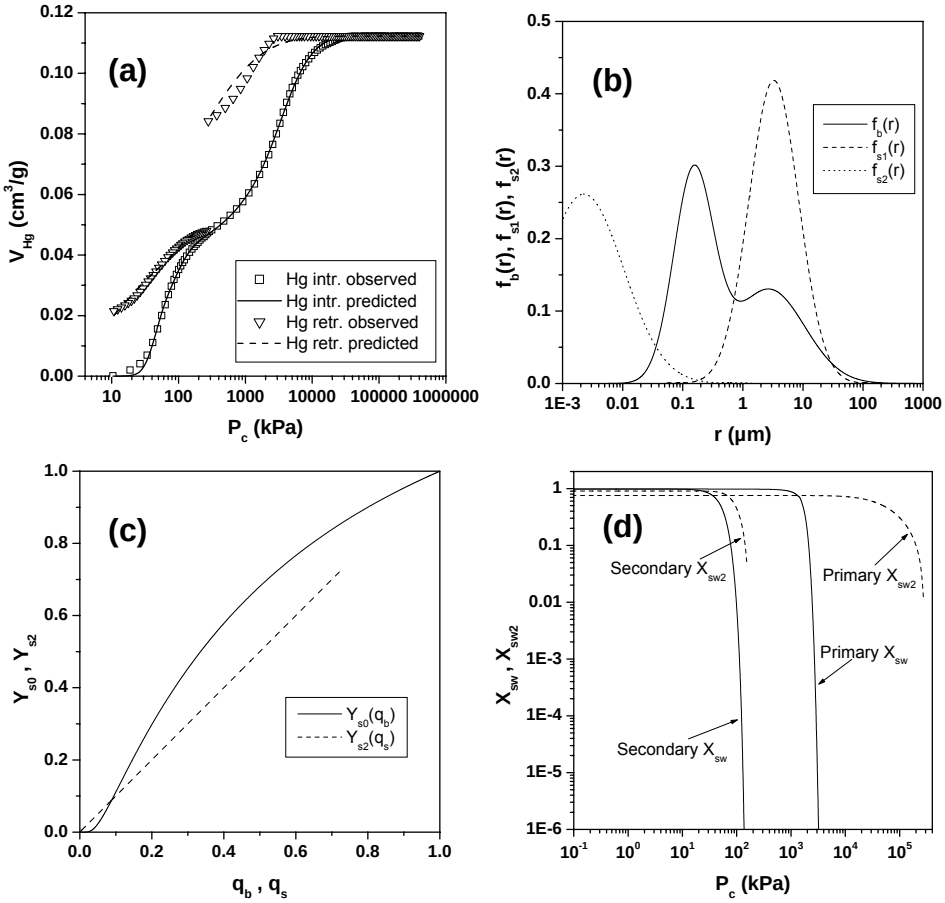

Figure 4. Pore structure properties of cj4. (a) Comparison of experimental to theoretically predicted Hg intrusion and retraction curves. (b) Estimated (number-based) PBRD and PTRD of the macroporosity and (number-based) PBRD of microporosity (c_s=1.76x10^{-7}). (c) Estimated DAFs (q_{bc0}=0.098). (d) Estimated IAFs

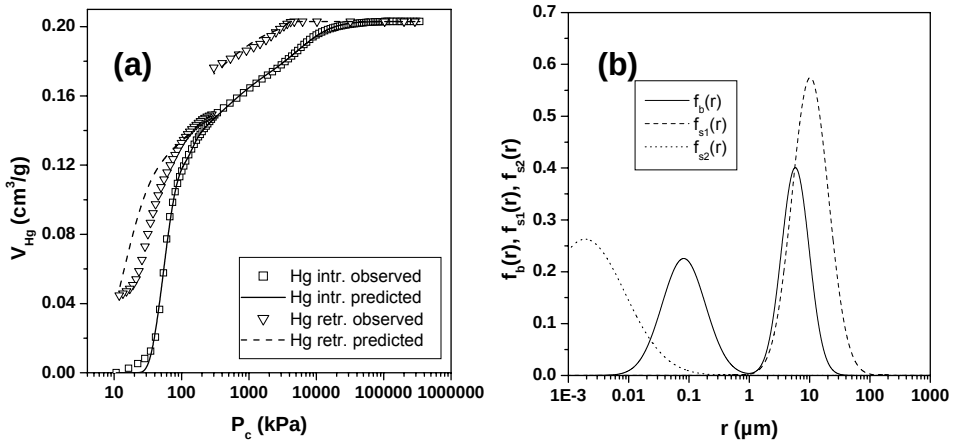

Figure 5. Pore structure properties of st-maximin. (a) Comparison of experimental to theoretically predicted Hg porosimetry curves. (b) Estimated PBRD and PTRD of the macroporosity and PBRD of microporosity (c_s=4.73x10^{-8}).

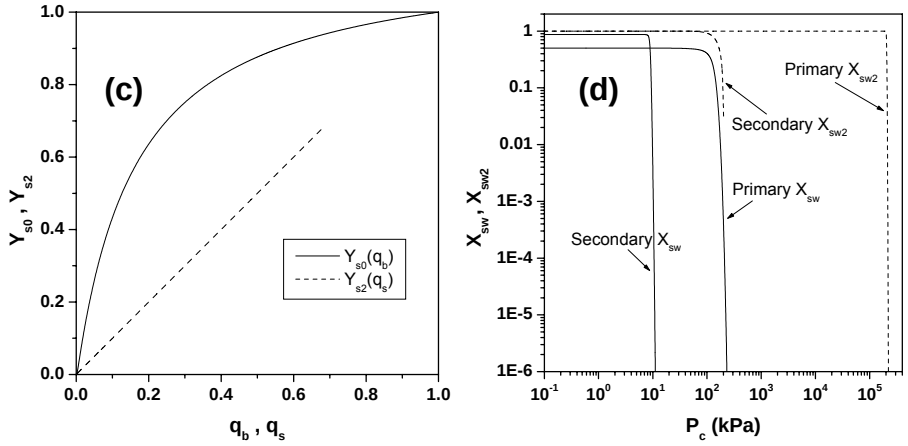

Figure 5 (cont'd). Pore structure properties of st-maximin. (c) Estimated DAFs (q_{bc0}=0.0075). (d) Estimated IAFs.

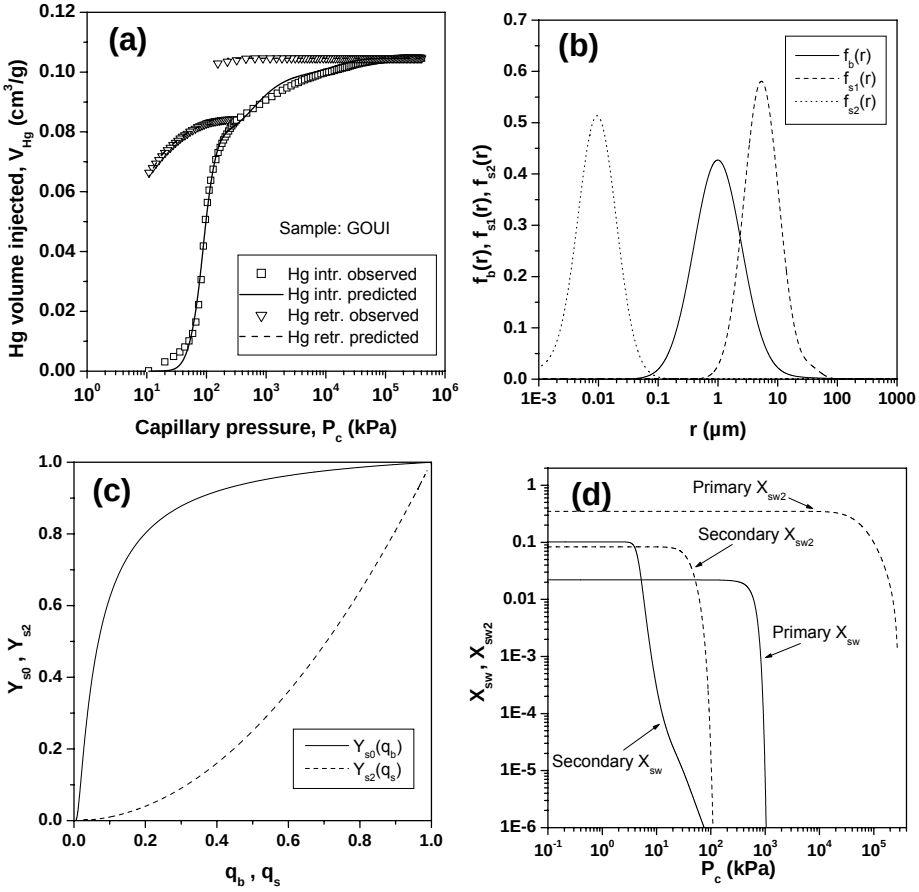

Figure 6. Pore structure properties of goui. (a) Comparison of experimental to theoretically predicted Hg intrusion and retraction curves. (b) Estimated PBRD and PTRD of the macroporosity and PBRD of microporosity (c_s=4.96x10^{-8}). (c) Estimated DAFs (q_{bc0}=0.02). (d) Estimated IAFs.